



Available online at www.sciencedirect.com



Appl. Comput. Harmon. Anal. 17 (2004) 259–276

**Applied and
Computational
Harmonic Analysis**

www.elsevier.com/locate/acha

3D discrete X-ray transform

Amir Averbuch*, Yoel Shkolnisky¹

School of Computer Science, Tel Aviv University, Tel Aviv 69978, Israel

Received 5 April 2003; revised 29 April 2004; accepted 12 May 2004

Available online 5 August 2004

Communicated by the Editors

Abstract

The analysis of 3D discrete volumetric data becomes increasingly important as computation power increases. 3D analysis and visualization applications are expected to be especially relevant in areas like medical imaging and nondestructive testing, where elaborated continuous theory exists. However, this theory is not directly applicable to discrete datasets. Therefore, we have to establish theoretical foundations that will replace the existing inexact discretizations, which have been based on the continuous regime. We want to preserve the concepts, properties, and main results of the continuous theory in the discrete case. In this paper, we present a discretization of the continuous X-ray transform for discrete 3D images. Our definition of the discrete X-ray transform is shown to be exact and geometrically faithful as it uses summation along straight geometric lines without arbitrary interpolation schemes. We derive a discrete Fourier slice theorem, which relates our discrete X-ray transform with the Fourier transform of the underlying image, and then use this Fourier slice theorem to derive an algorithm that computes the discrete X-ray transform in $O(n^4 \log n)$ operations. Finally, we show that our discrete X-ray transform is invertible. © 2004 Elsevier Inc. All rights reserved.

1. Introduction

The X-ray transform is an important practical tool in many scientific and industrial areas. An example of such area is computerized tomography (CT) scanning where the X-ray transform plays a major role

* Corresponding author.

E-mail address: amir@math.tau.ac.il (A. Averbuch).

¹ This work was supported by a grant from the Ministry of Science, Israel.

in the derivation and implementation of various tomographic methods. See [1] for an introduction to computerized tomography and the application of the X-ray transform to various tomographic methods.

1.1. The continuous X-ray transform

The continuous X-ray transform of a 3D function $f(x, y, z)$, denoted by $\mathcal{P}f$, is defined by the set of all line integrals of f . For a line L , defined by a unit vector θ and a point x on L , we express L as

$$L(t) = x + t\theta, \quad t \in \mathbb{R}. \quad (1.1)$$

The X-ray transform of f on L is defined as

$$\mathcal{P}f(L) \triangleq \int_{-\infty}^{\infty} f(x + t\theta) dt. \quad (1.2)$$

The X-ray transform maps each line L in \mathbb{R}^3 to a real value that represents the projection of the function f along the line L . For convenience, Eq. (1.2) is sometimes written with the notation

$$\mathcal{P}_\theta f(x) \triangleq \mathcal{P}f(L), \quad (1.3)$$

where L is given by Eq. (1.1).

The X-ray transform is closely related to the Radon transform. However, while the 3D X-ray transform is defined using line integrals of a function f , we define the 3D Radon transform as integrals of f over all planes in \mathbb{R}^3 . Note that in the 2D case, the X-ray transform coincides with the Radon transform. See [2–4] for more information about the continuous Radon transform.

1.2. The continuous Fourier slice theorem

The Fourier slice theorem connects the continuous X-ray transform, defined by Eq. (1.2), with the Fourier transform. For a given 3D function f , it defines the relation between the 2D Fourier transform of the X-ray transform of f and the 3D Fourier transform of f . The Fourier slice theorem is summarized in the following theorem.

Theorem 1.1. *For a function $f(x, y, z)$ and a family of lines in \mathbb{R}^3 , whose direction is given by the unit vector θ , it holds*

$$\widehat{\mathcal{P}_\theta f}(\xi) = \hat{f}(\xi), \quad (1.4)$$

where $\xi \in \theta^\perp$ and θ^\perp is the subspace perpendicular to θ .

1.3. Discretization guidelines

We define a 3D $n \times n \times n$ image as the set

$$I = \{I(u, v, w): -n/2 \leq u, v, w \leq n/2 - 1\}. \quad (1.5)$$

Note that we define I in Eq. (1.5) as a cube of voxels with an even side of length n . We refer to the image I as a cube of size $n \times n \times n$ to simplify the formulation of the discrete transform. The entire formulation can be repeated for an image I with arbitrary dimensions $n_1 \times n_2 \times n_3$.

As was done for the discretization of the Radon transform in [5], we are looking for a discrete definition of the X-ray transform for discrete images I that simultaneously satisfies the following properties: (P1) algebraic exactness, (P2) geometric fidelity, (P3) rapid computation algorithm, (P4) invertibility, and (P5) parallelism with the continuum theory. Detailed description of the properties (P1)–(P5) is given in [5].

In this paper we present a discrete definition of the 3D X-ray transform for discrete images, which satisfies the properties (P1)–(P5). We prove the Fourier slice theorem that relates our definition of the X-ray transform with the Fourier transform of the image I and develop a rapid computational algorithm, which is based on the Fourier slice theorem. We also show that our discrete X-ray transform is invertible.

The present work is based on [5] and [6]. However, there are important differences between them and the present work. [5] and [6] establish a framework for surface integrals decomposition of discrete objects. The present work derives a framework for line integrals decomposition of discrete objects. The two frameworks coincide for the 2D case, but for higher dimensions there are some fundamental differences between them. Although both frameworks follow the same guidelines and use the same building blocks, they require different discretizations of the continuous space because of the difference between the underlying continuous transforms. This results in a different frequency domain geometry, a different relation between the space domain and the frequency domain, and a different numerical computation algorithm.

The structure of the paper is as follows. In Section 2 we give a definition of the discrete X-ray transform, which defines transform for discrete images and a continuous set of lines in \mathbb{R}^3 . Section 3 establishes the fundamental Fourier slice theorem for our definition of the X-ray transform. In Section 4 we redefine the X-ray transform for both discrete images and a discrete set of lines in \mathbb{R}^3 , i.e., we discretize the set of lines given in the definition of the X-ray transform in Section 2. We show in Section 5 that for this special discrete set of lines the discrete X-ray transform is rapidly computable. Finally, in Section 6 we show that our discrete X-ray transform is invertible.

2. Semi-discrete transform definition

We parameterize a line in \mathbb{R}^3 as the intersection of two planes. Using this parameterization we define three families of lines, which we call x -lines, y -lines, and z -lines. Formally, a x -line is defined as

$$l_x(\alpha, \beta, c_1, c_2) = \begin{cases} y = \alpha x + c_1, \\ z = \beta x + c_2, \end{cases} \quad |\alpha| \leq 1, |\beta| \leq 1, c_1, c_2 \in \{-n, \dots, n\}. \quad (2.1)$$

Figure 1 is a 3D illustration of the family of x -lines that corresponds to $c_1 = c_2 = 0$, together with its projections on different axes. Similarly, a y -line and a z -line are defined as

$$l_y(\alpha, \beta, c_1, c_2) = \begin{cases} x = \alpha y + c_1, \\ z = \beta y + c_2, \end{cases} \quad |\alpha| \leq 1, |\beta| \leq 1, c_1, c_2 \in \{-n, \dots, n\}, \quad (2.2)$$

$$l_z(\alpha, \beta, c_1, c_2) = \begin{cases} x = \alpha z + c_1, \\ y = \beta z + c_2, \end{cases} \quad |\alpha| \leq 1, |\beta| \leq 1, c_1, c_2 \in \{-n, \dots, n\}. \quad (2.3)$$

We denote the sets of all x -lines, y -lines, and z -lines in \mathbb{R}^3 by \mathcal{L}_x , \mathcal{L}_y , and \mathcal{L}_z , respectively. Also, we denote the family of lines that corresponds to a fixed direction (α, β) and variable intercepts (c_1, c_2) , by $l_x(\alpha, \beta)$, $l_y(\alpha, \beta)$, and $l_z(\alpha, \beta)$ for a family of x -lines, y -lines, and z -lines, respectively. See Fig. 2 for an illustration of the different families of lines for $c_1 = c_2 = 0$.

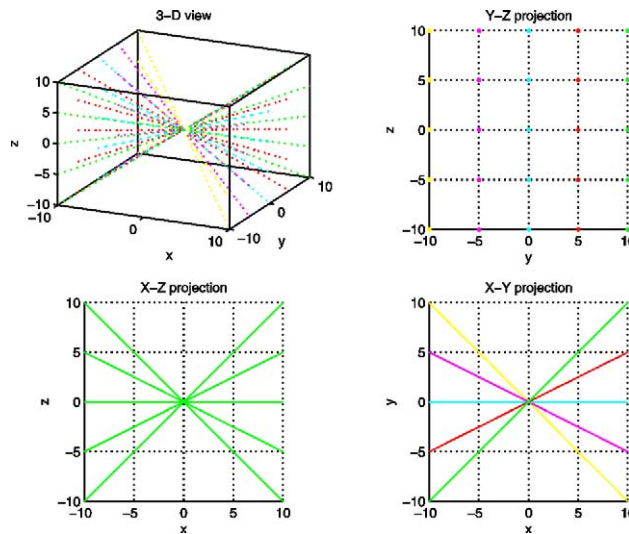


Fig. 1. The set of x -lines \mathcal{L}_x .

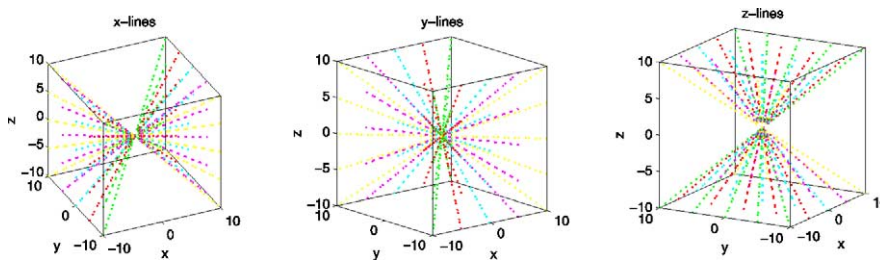


Fig. 2. The line families \mathcal{L}_x , \mathcal{L}_y , and \mathcal{L}_z .

It is easy to see that each line in \mathbb{R}^3 can be expressed as either a x -line, y -line, or z -line. In other words, each line in \mathbb{R}^3 belongs to \mathcal{L}_x , \mathcal{L}_y , or \mathcal{L}_z . Note that the sets \mathcal{L}_x , \mathcal{L}_y , and \mathcal{L}_z are not disjoint.

Generally speaking, for a given image I and a line l , we define the discrete X-ray transform of the image I for the line l as the sum of the samples of I along l . Since the image I is discrete, we must carefully select a continuous extension of I in order to compute the samples of I along l . As we will see, there exists an extension scheme that enables us to define the discrete X-ray transform while satisfying properties (P1)–(P5) from Section 1.3.

For a discrete image I of size $n \times n \times n$ we define three continuous extensions of I , which we denote by I_x , I_y , and I_z . Each of the extensions I_x , I_y , and I_z is a continuous function in the directions perpendicular to its index. This means, for example, that I_x is a continuous function in the y and z directions. Formally, we define these three extensions by

$$I_x(u, y, z) = \sum_{v=-n/2}^{n/2-1} \sum_{w=-n/2}^{n/2-1} I(u, v, w) D_m(y-v) D_m(z-w),$$

$$u \in \{-n/2, \dots, n/2-1\}, y, z \in \mathbb{R}, \tag{2.4}$$

$$I_y(x, v, z) = \sum_{u=-n/2}^{n/2-1} \sum_{w=-n/2}^{n/2-1} I(u, v, w) D_m(x-u) D_m(z-w),$$

$$v \in \{-n/2, \dots, n/2-1\}, x, z \in \mathbb{R}, \tag{2.5}$$

$$I_z(x, y, w) = \sum_{u=-n/2}^{n/2-1} \sum_{v=-n/2}^{n/2-1} I(u, v, w) D_m(x-u) D_m(y-v),$$

$$w \in \{-n/2, \dots, n/2-1\}, x, y \in \mathbb{R}, \tag{2.6}$$

where D_m is the Dirichlet kernel of length $m = 2n + 1$ given by

$$D_m(t) = \frac{\sin \pi t}{m \sin(\pi t/m)}. \tag{2.7}$$

The Dirichlet kernel, given by Eq. (2.7), performs trigonometric interpolation of length m . Therefore, the continuous functions I_x , I_y , and I_z are obtained from the discrete image I by zero padding the relevant directions of I to length m and then performing trigonometric interpolation. The length m of the interpolatory kernel D_m is critical and its selection will be described below.

Next, we use I_x , I_y , and I_z to define the discrete X-ray transform. For a x -line $l_x(\alpha, \beta, c_1, c_2) \in \mathcal{L}_x$, given by Eq. (2.1), we define the discrete X-ray transform $P_x I(\alpha, \beta, c_1, c_2)$ as

$$P_x I(\alpha, \beta, c_1, c_2) = \sum_{u=-n/2}^{n/2-1} I_x(u, \alpha u + c_1, \beta u + c_2)$$

$$|\alpha| \leq 1, |\beta| \leq 1, c_1, c_2 \in \{-n, \dots, n\}, \tag{2.8}$$

where I_x is given by Eq. (2.4). The transformation $P_x : \mathcal{L}_x \rightarrow \mathbb{R}$ is obtained by traversing the line l_x with unit steps in the x direction, and for each integer u the value of the image I at the point $(u, \alpha u + c_1, \beta u + c_2)$ is summed.

The parameters c_1 , c_2 , and m in Eqs. (2.1) and (2.4) are carefully chosen to ensure that the transform, defined by Eq. (2.8), is invertible and geometrically faithful. We begin by inspecting the selection of the parameters c_1 and c_2 . The transform in Eq. (2.8) must be defined over all lines that intersect the image I . Since the slopes α and β are limited to the interval $[-1, 1]$, one can easily verify that it is sufficient to select $c_1, c_2 \in \{-n, \dots, n\}$. For example, if we set $\alpha = \beta = -1$, then for $c_1 = c_2 = -n$, the x -line that is given by the parameters $(\alpha, \beta, c_1, c_2)$ intersects I at a single point $(-n/2, -n/2, -n/2)$. For values of c_1 and c_2 smaller than $-n$, the line does not intersect I , and, therefore, it is ignored. To conclude, for the family of x -lines, defined by Eq. (2.1), it is sufficient to select $c_1, c_2 \in \{-n, \dots, n\}$. Note that although the set of values for c_1 and c_2 is discrete, the set of x -lines \mathcal{L}_x is continuous since the slopes α and β are continuous. Therefore, to obtain a fully discrete definition of the X-ray transform we have to discretize the set \mathcal{L}_x , i.e., the slopes α and β . We will handle this discretization in Section 4.

We choose $m \geq 2n + 1$ as the length of the interpolation kernel D_m to avoid line wraparound due to the periodic nature of the Dirichlet kernel. Loosely speaking, using a kernel shorter than $2n + 1$ causes the samples of I_x along a line l_x at points with (for example) z value greater than $n/2$ to coincide with the samples of I_x with $-n/2 \leq z \leq n/2$. Geometrically, this is interpreted as a wraparound of the line l_x . To avoid this wraparound and to achieve a summation over true geometric lines, we select $m \geq 2n + 1$. Hence, $m = 2n + 1$ is the shortest kernel that satisfies property (P2) from Section 1.3. See [5] for a rigorous derivation of the length of the shortest valid kernel.

Similarly to Eq. (2.8), we define the discrete X-ray transform $P_y I(\alpha, \beta, c_1, c_2)$ for the y -line $l_y(\alpha, \beta, c_1, c_2) \in \mathcal{L}_y$ as

$$P_y I(\alpha, \beta, c_1, c_2) = \sum_{v=-n/2}^{n/2-1} I_y(\alpha v + c_1, v, \beta v + c_2), \quad (2.9)$$

where I_y is given by Eq. (2.5). Finally, we define the discrete X-ray transform $P_z I(\alpha, \beta, c_1, c_2)$ for a z -line $l_z(\alpha, \beta, c_1, c_2) \in \mathcal{L}_z$ as

$$P_z I(\alpha, \beta, c_1, c_2) = \sum_{w=-n/2}^{n/2-1} I_z(\alpha w + c_1, \beta w + c_2, w), \quad (2.10)$$

where I_z is given by Eq. (2.6).

Equations (2.8)–(2.10) define the X-ray transform for x -lines, y -lines, and z -lines, respectively. Since each line in \mathbb{R}^3 can be expressed as either a x -line, y -line, or z -line, then, given a line l , we express it as either a x -line, y -line, or z -line and apply on it our definition of the X-ray transform. Hence, for a given image I and a line l , we define the discrete X-ray transform of I for the line l as

Definition 2.1.

$$PI(l) = \begin{cases} P_x I(l), & l \in \mathcal{L}_x, \\ P_y I(l), & l \in \mathcal{L}_y, \\ P_z I(l), & l \in \mathcal{L}_z. \end{cases} \quad (2.11)$$

There is a subtle difference between the continuous X-ray transform, given in Eq. (1.2), and the discrete X-ray transform, given in Eq. (2.11). The continuous X-ray transform assigns to each line the integral of the object along the line, where the value of the integral is independent of the parameterization of the line. The discrete X-ray transform assigns a value to a specific parameterization of the line. This means that if the same line is written in two different ways in Eq. (2.11), then, it may receive two different values. This problem occurs only for lines that have an angle of 45° in some direction. We can eliminate this problem by using a more subtle construction in Eq. (2.11). However, since this issue does not pose any computational problems, we simply ignore it.

The X-ray transform, given by Definition 2.1, is defined for a set of lines in \mathbb{R}^3 with a discrete set of intercepts (c_1, c_2) and a continuous set of slopes (α, β) . Therefore, Definition 2.1 is what we call “semi-discrete,” since it is discrete with respect to the image I and the set of intercepts (c_1, c_2) , but it uses a continuous set of slopes (α, β) . In Section 4 we show how to discretize the set (α, β) to have a fully discrete definition of the X-ray transform, which is rapidly computable and invertible.

3. Discrete Fourier slice theorem for the discrete X-ray transform

As we showed in Eq. (1.4), the continuous X-ray transform satisfies the Fourier slice theorem, which associates the continuous X-ray transform of a function f with the Fourier transform of f . This relation is very useful for both the computation and analysis of the continuous X-ray transform. We will, therefore, derive a similar relation for the discrete X-ray transform, and we will later utilize it to rapidly compute the discrete X-ray transform.

For a 2D array X of size $m \times m$ ($m = 2n + 1$), the 2D discrete Fourier transform (DFT) of X , denoted by \widehat{X} , is defined by

$$\widehat{X}(k, l) = \sum_{u=-n}^n \sum_{v=-n}^n X(u, v) e^{-2\pi i k u / m} e^{-2\pi i l v / m}, \quad k, l = -n, \dots, n. \tag{3.1}$$

The 2D inverse discrete Fourier transform is given by

$$X(u, v) = \sum_{k=-n}^n \sum_{l=-n}^n \widehat{X}(k, l) e^{2\pi i k u / m} e^{2\pi i l v / m}, \quad u, v = -n, \dots, n. \tag{3.2}$$

Given a family of x -lines $l_x(\alpha, \beta)$, we denote the X-ray transform of the image I for this family of lines by $P_{x(\alpha, \beta)} I$. Formally,

$$P_{x(\alpha, \beta)} I \triangleq P_x I(\alpha, \beta, c_1, c_2), \quad c_1, c_2 = -n, \dots, n \tag{3.3}$$

or for specific c_1 and c_2 ,

$$P_{x(\alpha, \beta)} I(c_1, c_2) \triangleq P_x I(\alpha, \beta, c_1, c_2), \tag{3.4}$$

where $P_x I(\alpha, \beta, c_1, c_2)$ is given by Eq. (2.8). $P_{x(\alpha, \beta)} I$ is the 2D array generated by applying the X-ray transform to a family of x -lines with a fixed direction (α, β) .

We will inspect the 2D discrete Fourier transform of the array $P_{x(\alpha, \beta)} I$. The 2D DFT of the array $P_{x(\alpha, \beta)} I$ is given by

$$\widehat{P}_{x(\alpha, \beta)} I(k, l) = \sum_{u, v=-n}^n P_{x(\alpha, \beta)} I(u, v) e^{-2\pi i k c_1 / m} e^{-2\pi i l c_2 / m} \tag{3.5}$$

$$= \sum_{u, v=-n}^n \sum_{x, y, z=-n/2}^{n/2-1} I(x, y, z) D_m(\alpha x + u - y) D_m(\beta x + v - z) e^{-2\pi i k u / m} e^{-2\pi i l v / m}$$

(by Eq. (2.4))

$$\tag{3.6}$$

$$= \sum_{x, y, z=-n/2}^{n/2-1} I(x, y, z) \left(\sum_{u=-n}^n D_m(\alpha x + u - y) e^{-2\pi i k u / m} \right) \times \left(\sum_{v=-n}^n D_m(\beta x + v - z) e^{-2\pi i l v / m} \right). \tag{3.7}$$

To analyze the term $\sum_{u=-n}^n D_m(\alpha x + u - y) e^{-2\pi i k u / m}$, given in Eq. (3.7), we use the *translation operator*, given in [5], and define it by

$$T_\tau \alpha : \mathbb{C}^m \rightarrow \mathbb{C}^m, \quad m = 2n + 1, \quad \tau \in \mathbb{R} \quad (T_\tau \alpha)(u) = \sum_{j=-n}^n \alpha_j D_m(\tau + j - u). \tag{3.8}$$

Lemma 3.1 [5]. *Let $m = 2n + 1$, $\varphi_k(x) = e^{2\pi i k x / m}$. Define the vector $\phi_k \in \mathbb{C}^m$ by $\phi_k(u) = \varphi_k(u)$, $u = -n, \dots, n$. Then, for an arbitrary $\tau \in \mathbb{R}$ and $v = -n, \dots, n$ we have $(T_\tau \phi_k)(v) = \varphi_k(v - \tau)$.*

If we denote by $\phi_k(u)$ the vector $\phi_k = (e^{-2\pi iku/m})$, $u = -n, \dots, n$, then, by using Eq. (3.8) we can write

$$\sum_{u=-n}^n D_m(\alpha x + u - y)e^{-2\pi iku/m} = (T_{\alpha x}\phi_k)_y. \tag{3.9}$$

Since ϕ_k is a vector of samples of the exponential $\varphi_k(x) = e^{-2\pi ikx/m}$, then, by Lemma 3.1 we have

$$(T_{\alpha x}\phi_k)_y = \varphi(y - \alpha x) = e^{-2\pi ik(y-\alpha x)/m}. \tag{3.10}$$

Substituting Eq. (3.10) in Eq. (3.9) we get

$$\sum_{u=-n}^n D_m(\alpha x + u - y)e^{-2\pi iku/m} = e^{-2\pi ik(y-\alpha x)/m}. \tag{3.11}$$

Similarly, for the term $\sum_{v=-n}^n D_m(\beta x + v - z)e^{-2\pi ilv/m}$, given in Eq. (3.7), it follows that:

$$\sum_{v=-n}^n D_m(\beta x + v - z)e^{-2\pi ilv/m} = e^{-2\pi il(z-\beta x)/m}. \tag{3.12}$$

Combining Eqs. (3.11) and (3.12) into Eq. (3.7) we obtain

$$\widehat{P}_{x(\alpha,\beta)}I(k, l) = \sum_{u,v,w=-n/2}^{n/2-1} I(u, v, w)e^{-2\pi ik(v-\alpha u)/m}e^{-2\pi il(w-\beta u)/m} \tag{3.13}$$

$$= \sum_{u,v,w=-n/2}^{n/2-1} I(u, v, w)e^{-2\pi iu(-\alpha k-\beta l)/m}e^{-2\pi ikv/m}e^{-2\pi ilw/m} \tag{3.14}$$

$$= \widehat{I}(-\alpha k - \beta l, k, l), \tag{3.15}$$

where \widehat{I} is the trigonometric polynomial defined by

$$\widehat{I}(\xi_1, \xi_2, \xi_3) = \sum_{u=-n/2}^{n/2-1} \sum_{v=-n/2}^{n/2-1} \sum_{w=-n/2}^{n/2-1} I(u, v, w)e^{-2\pi i\xi_1u/m}e^{-2\pi i\xi_2v/m}e^{-2\pi i\xi_3w/m}. \tag{3.16}$$

We just proved the following theorem.

Theorem 3.2 (*x*-Lines Fourier slice theorem). *For a given family of x-lines $l_x(\alpha, \beta)$ with fixed slopes (α, β) and variable intercepts (c_1, c_2) , we take the 2D array of projections $P_{x(\alpha,\beta)}I$. Then,*

$$\widehat{P}_{x(\alpha,\beta)}I(k, l) = \widehat{I}(-\alpha k - \beta l, k, l), \tag{3.17}$$

where \widehat{I} is given by Eq. (3.16) and $\widehat{P}_{x(\alpha,\beta)}I(k, l)$ is the 2D DFT of the array $P_{x(\alpha,\beta)}I$.

Similar theorems hold for *y*-lines and *z*-lines.

Geometrically, Theorem 3.2 states that the 2D DFT of the discrete X-ray transform over a family of *x*-lines with fixed slopes (α, β) is equal to the samples of the trigonometric polynomial \widehat{I} on the plane defined by the points $(-\alpha k - \beta l, k, l)$. Explicitly, we need to sample \widehat{I} on the plane given by the equation $x = -\alpha y - \beta z$. Figure (3) depicts these *x*-planes for various values of α and β . Theorem 3.2 is very important for the rapid computation of the discrete X-ray transform, as it relates the discrete X-ray transform of the image I to the 3D DFT of I .

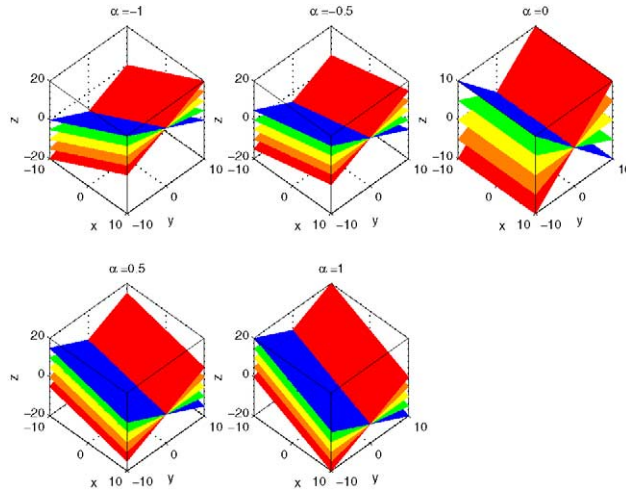


Fig. 3. x -planes for various values of α and β .

4. Discretization of the X-ray transform

Definition 2.1 defines the X-ray transform over the continuous line sets \mathcal{L}_x , \mathcal{L}_y , and \mathcal{L}_z . These line sets are comprised from lines that have discrete intercepts and continuous slopes. In this section we define the discrete X-ray transform for a discrete set of lines, which are discrete both in their slopes and intercepts.

Consider the set defined by

$$S = \{2p/n\}, \quad p = -n/2, \dots, n/2. \tag{4.1}$$

We define the *discrete X-ray transform* as the restriction of Definition 2.1 to the set of slopes $S \times S$. Formally, we define three discrete sets of lines:

- discrete x -lines

$$\mathcal{L}_x^d = \{l_x(\alpha, \beta, c_1, c_2) \in \mathcal{L}_x \mid \alpha \in S, \beta \in S\}, \tag{4.2}$$

- discrete y -lines

$$\mathcal{L}_y^d = \{l_y(\alpha, \beta, c_1, c_2) \in \mathcal{L}_y \mid \alpha \in S, \beta \in S\}, \tag{4.3}$$

- discrete z -lines

$$\mathcal{L}_z^d = \{l_z(\alpha, \beta, c_1, c_2) \in \mathcal{L}_z \mid \alpha \in S, \beta \in S\}. \tag{4.4}$$

The set \mathcal{L}^d is defined by

$$\mathcal{L}^d = \mathcal{L}_x^d \cup \mathcal{L}_y^d \cup \mathcal{L}_z^d. \tag{4.5}$$

By using the lines in \mathcal{L}^d we define the discrete X-ray transform for discrete images as

Definition 4.1. For an image I and a line $l(\alpha, \beta, c_1, c_2) \in \mathcal{L}^d$ the discrete X-ray transform is given by

$$PI(l) = \begin{cases} P_x I(l), & l \in \mathcal{L}_x^d, \\ P_y I(l), & l \in \mathcal{L}_y^d, \\ P_z I(l), & l \in \mathcal{L}_z^d, \end{cases} \quad (4.6)$$

where P_x , P_y , and P_z are defined by Eqs. (2.8)–(2.10), respectively.

Definition 4.1 defines the discrete X-ray transform for discrete images by using a discrete set of lines. This transform is not defined for all lines in \mathbb{R}^3 , but only for lines in \mathcal{L}^d . We will show in Section 5 that for the set of lines \mathcal{L}^d the discrete X-ray transform can be computed using a fast algorithm. Moreover, we will show in Section 6 that the discrete X-ray transform is invertible.

Since the Fourier slice Theorem 3.2 holds for continuous slopes (α, β) , it holds in particular for the discrete set of slopes defined by Eq. (4.1). Substituting the discrete set of slopes, given by Eq. (4.1), into Theorem 3.2 gives the discrete Fourier slice theorem, which is defined for both discrete images and a discrete set of directions.

Corollary 4.1 (Discrete Fourier slice theorem). *Let S be the set given in Eq. (4.1) and let \hat{I} be the trigonometric polynomial defined by*

$$\hat{I}(\xi_1, \xi_2, \xi_3) = \sum_{u=-n/2}^{n/2-1} \sum_{v=-n/2}^{n/2-1} \sum_{w=-n/2}^{n/2-1} I(u, v, w) e^{-2\pi i \xi_1 u/m} e^{-2\pi i \xi_2 v/m} e^{-2\pi i \xi_3 w/m}. \quad (4.7)$$

Then,

- For a given family of x -lines $l_x(\alpha, \beta)$, $\alpha = 2p/n \in S_1$, $\beta = 2q/n \in S_2$,

$$\hat{P}_{x(2p/n, 2q/n)} I(k, l) = \hat{I}(-2pk/n - 2ql/n, k, l). \quad (4.8)$$

- For a given family of y -lines $l_y(\alpha, \beta)$, $\alpha = 2p/n \in S_1$, $\beta = 2q/n \in S_2$,

$$\hat{P}_{y(2p/n, 2q/n)} I(k, l) = \hat{I}(k, -2pk/n - 2ql/n, l). \quad (4.9)$$

- For a given family of z -lines $l_z(\alpha, \beta)$, $\alpha = 2p/n \in S_1$, $\beta = 2q/n \in S_2$,

$$\hat{P}_{z(2p/n, 2q/n)} I(k, l) = \hat{I}(k, l, -2pk/n - 2ql/n). \quad (4.10)$$

5. Computing the discrete X-ray transform

Equation (4.6) shows that direct computation of the discrete X-ray transform according to its definition requires $O(n^7)$ operations. As we will shortly see, by utilizing the frequency domain relations between the samples of the discrete X-ray transform, it is possible to compute it in $O(n^4 \log n)$ operations without sacrificing the accuracy. This is quite a remarkable result if we consider the fact that the lower bound for such a computation is $\Omega(n^4)$ operations, since there are four independent parameters $(\alpha, \beta, c_1, c_2)$ to consider.

We consider only the computation of the discrete X-ray transform for \mathcal{L}_x^d , given by Eq. (4.2). The algorithm for computing the discrete X-ray transform for \mathcal{L}_y^d and \mathcal{L}_z^d is similar. The discrete Fourier slice theorem for a x -line l_x (Eq. (4.8)) is given by

$$\widehat{P}_{x(2p/n, 2q/n)} I(k, l) = \widehat{I}(-2pk/n - 2ql/n, k, l), \quad p, q \in \{n/2, \dots, n/2\}. \tag{5.1}$$

If we can rapidly sample the trigonometric polynomial \widehat{I} , given by Eq. (3.16), at the points $(-2pk/n - 2ql/n, k, l)$ for some fixed p and q , then, by the 2D inverse DFT we can recover the values of $P_{x(2p/n, 2q/n)} I(c_1, c_2)$ for fixed p and q . Hence, once we compute the samples $\widehat{P}_{x(2p/n, 2q/n)} I(k, l)$ for all possible values of p, q, k , and l , it requires $(n + 1)^2$ applications of the 2D inverse DFT (one for each pair of p and q) to recover $P_x I$ for all x -lines $l_x \in \mathcal{L}_x^d$. This results in a total of $O(n^4 \log n)$ operations to recover $P_x I$ from $\widehat{P}_x I$. Therefore, remains to show that we can compute $\widehat{P}_{x(2p/n, 2q/n)} I(k, l)$ for all p, q, k , and l using $O(n^4 \log n)$ operations.

We take some fixed slope $\alpha = 2p/n \in S$ and denote

$$\widehat{I}_p(q, k, l) = \widehat{I}(-2pk/n - 2ql/n, k, l), \tag{5.2}$$

where \widehat{I} is given by Eq. (3.16). By expanding Eq. (5.2) using Eq. (3.16) we obtain

$$\widehat{I}_p(q, k, l) = \widehat{I}(-2pk/n - 2ql/n, k, l) \tag{5.3}$$

$$= \sum_{u, v, w = -n/2}^{n/2-1} I(u, v, w) e^{-2\pi i u(-2pk/n - 2ql/n)/m} e^{-2\pi i kv/m} e^{-2\pi i lw/m}. \tag{5.4}$$

Denote

$$\widehat{I}_{yz}(u, k, l) = \sum_{v = -n/2}^{n/2-1} \sum_{w = -n/2}^{n/2-1} I(u, v, w) e^{-2\pi i kv/m} e^{-2\pi i lw/m}. \tag{5.5}$$

By substituting Eq. (5.5) into Eq. (5.4) we obtain

$$\widehat{I}_p(q, k, l) = \sum_{u = -n/2}^{n/2-1} \widehat{I}_{yz}(u, k, l) e^{-2\pi i u(-2pk/n - 2ql/n)/m} \tag{5.6}$$

or

$$\widehat{I}_p(q, k, l) = \sum_{u = -n/2}^{n/2-1} \widehat{I}_{yz}(u, k, l) e^{-2\pi i u \omega_q}, \tag{5.7}$$

where

$$\Delta\omega = -2l/(nm), \quad \omega_0 = -2pk/(nm), \quad \omega_q = \omega_0 + q \Delta\omega. \tag{5.8}$$

If we compute $\widehat{I}_p(q, k, l)$, given in Eq. (5.7), for all values of q, k , and l , then, by Eqs. (5.2) and (5.1) we can compute $\widehat{P}_{x(2p/n, 2q/n)} I(k, l)$ for a fixed direction p . Repeating the process for all possible values of p produces the values of $\widehat{P}_{x(2p/n, 2q/n)} I(k, l)$ for all possible p, q, k , and l . Hence, rapid evaluation of Eq. (5.7) enables rapid computation of the discrete X-ray transform.

Equations (5.7) and (5.8) reveal a special relation between the samples of $\widehat{I}_p(q, k, l)$. As we will see in Section 5.1, we can utilize this relation to rapidly compute the values of $\widehat{I}_p(q, k, l)$ by using the chirp Z-transform. We first introduce the chirp Z-transform, and later show how to use it to rapidly compute the discrete X-ray transform.

5.1. The chirp Z-transform

Given a sequence $x(j)$, $j = -n/2, \dots, n/2 - 1$, its Z-transform is defined by

$$X(z) = \sum_{j=-n/2}^{n/2-1} x(j)z^{-j}. \quad (5.9)$$

The chirp Z-transform, first discussed in [7], rapidly computes $X(z_k)$ for points $z_k = AW^{-k}$, where $A, W \in \mathbb{C}$. Specifically, the chirp Z-transform allows to compute $X(z_k)$ along contours of the form

$$z_k = e^{2\pi i \omega_k}, \quad \omega_k = \omega_0 + k\Delta\omega, \quad k = -n/2, \dots, n/2, \quad (5.10)$$

where ω_0 is an arbitrary starting frequency and $\Delta\omega$ is an arbitrary frequency increment. See Fig. 4 for an illustration of z_k defined by Eq. (5.10). For the contour defined by Eq. (5.10), the chirp Z-transform has the form

$$X(e^{2\pi i \omega_k}) = \sum_{j=-n/2}^{n/2-1} x(j)e^{-2\pi i j \omega_k}, \quad k = -n/2, \dots, n/2. \quad (5.11)$$

For the case where $\omega_0 = 0$ and $\Delta\omega = 1/n$, the chirp Z-transform in Eq. (5.11) computes the discrete Fourier transform of the sequence $x(j)$.

The algorithm described in [7–9] computes the chirp Z-transform of a sequence $x(j)$ of length n and arbitrary ω_0 and $\Delta\omega$ using $O(n \log n)$ operations.

Equations (5.7) and (5.8) state that for fixed k and l , $\hat{I}_p(q, k, l)$ can be rapidly computed by setting

$$x(j) = \hat{I}_{yz}(j, k, l), \quad \omega_0 = -2pk/(nm), \quad \Delta\omega = -2l/(nm) \quad (5.12)$$

and using the chirp Z-transform. These settings are used in the next section for the rapid computation of the discrete X-ray transform.

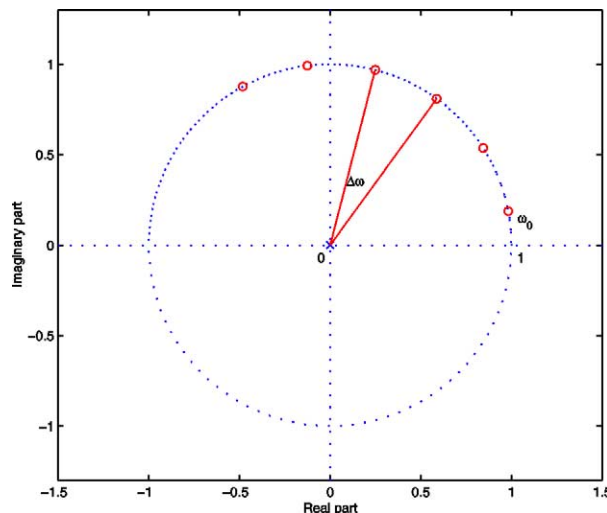


Fig. 4. Z-plane samples of the chirp Z-transform

5.2. Fast algorithm for the computation of the discrete X-ray transform

We will use the chirp Z-transform algorithm from Section 5.1 to rapidly compute $\widehat{P}I(l)$ for all $l \in \mathcal{L}^d$, where \mathcal{L}^d is defined in Eq. (4.5). The algorithm consists of three phases, which compute $\widehat{P}_x I$, $\widehat{P}_y I$, and $\widehat{P}_z I$ for lines in \mathcal{L}_x^d , \mathcal{L}_y^d , and \mathcal{L}_z^d , respectively. We present only the algorithm for computing $\widehat{P}_x I$. The algorithms for $\widehat{P}_y I$ and $\widehat{P}_z I$ are similar.

We use the following notation in the description of the algorithm:

- E_y, E_z —Extension operators, which symmetrically zero-pad the image I to length $2n + 1$ along the y and z directions, respectively.
- F_y, F_z —1D discrete Fourier transform (FFT) along the specified direction. For example, $F_y I$ takes all the vectors $I(x, \cdot, z)$ and applies on them the 1D FFT.
- $CZT(x, \omega_0, \Delta\omega)$ —The chirp Z-transform, defined in Section 5.1, with parameters ω_0 and $\Delta\omega$. Specifically, $CZT(x, \omega_0, \Delta\omega)$ is defined by

$$CZT(x, \omega_0, \Delta\omega)_k = \sum_{j=-n/2}^{n/2-1} x(j)e^{-2\pi i j \omega_k}, \quad \omega_k = \omega_0 + k\Delta\omega, \quad k = -n/2, \dots, n/2. \quad (5.13)$$

5.2.1. Algorithm description

The output of the algorithm is stored in the array Res_x of size $(n + 1) \times (n + 1) \times m \times m$, ($m = 2n + 1$).

- Computing $\widehat{P}_x I$:
 1. $\dot{I} = E_y E_z I$
 2. $\tilde{I} = F_y F_z \dot{I}$
 3. foreach p in $-n/2, \dots, n/2$
 4. foreach k, l in $-n, \dots, n$
 5. $x_{k,l} \leftarrow \tilde{I}(\cdot, k, l)$ ($x_{k,l}$ is a sequence of length n)
 6. $\omega_0 \leftarrow -2pk/(nm), \quad \Delta\omega \leftarrow -2l/(nm)$
 7. $\text{Res}_x(p, \cdot, k, l) = CZT(x_{k,l}, \omega_0, \Delta\omega)$
 8. endfor
 9. endfor

5.2.2. Correctness of Algorithm 5.1

Theorem 5.1. Upon termination of Algorithm 5.2.1 we have

$$\text{Res}_x(p, q, k, l) = \widehat{P}_{x(2p/n, 2q/n)} I(k, l).$$

Proof. According to step 2 of Algorithm 5.2.1, and the definitions of \hat{I} and F_z it follows that:

$$(F_z \hat{I})(u, v, l) = \sum_{w=-n}^n \hat{I}(u, v, w) e^{-2\pi i l w/m} = \sum_{w=-n/2}^{n/2-1} I(u, v, w) e^{-2\pi i l w/m}, \quad m = 2n + 1. \quad (5.14)$$

Applying F_y to Eq. (5.14) yields

$$\tilde{I}(u, k, l) \triangleq F_y(F_z \dot{I})(u, k, l) = \sum_{v=-n}^n F_z \dot{I}(u, v, l) e^{-2\pi i k v / m} \quad (5.15)$$

$$= \sum_{v=-n}^n \sum_{w=-n/2}^{n/2-1} I(u, v, w) e^{-2\pi i k v / m} e^{-2\pi i l w / m} \quad (5.16)$$

$$= \sum_{v=-n/2}^{n/2-1} \sum_{w=-n/2}^{n/2-1} I(u, v, w) e^{-2\pi i k v / m} e^{-2\pi i l w / m}. \quad (5.17)$$

According to step 5 of Algorithm 5.2.1 and Eq. (5.17), we define the sequence $\{x_{k,l}\}$ as

$$x_{k,l}(j) = \tilde{I}(j, k, l) = \sum_{v=-n/2}^{n/2-1} \sum_{w=-n/2}^{n/2-1} I(j, v, w) e^{-2\pi i k v / m} e^{-2\pi i l w / m}. \quad (5.18)$$

By applying the *CZT* (step 7) to $\{x_{k,l}\}$, given in Eq. (5.18), with parameters ω_0 and $\Delta\omega$, defined in step 6 of Algorithm 5.2.1, we obtain

$$\text{Res}_x(p, q, k, l) = \text{CZT}(x_{k,l}, \omega_0, \Delta\omega)_q \quad (5.19)$$

$$= \sum_{j=-n/2}^{n/2-1} x_{k,l}(j) z_q^{-j} \Big|_{z_q = e^{2\pi i \omega_q}} \quad (5.20)$$

$$= \sum_{j=-n/2}^{n/2-1} x_{k,l}(j) e^{-2\pi i j \omega_q} \quad (5.21)$$

$$= \sum_{j=-n/2}^{n/2-1} x_{k,l}(j) e^{-2\pi i j (\omega_0 + q \Delta\omega)} \quad (\text{since } \omega_q = \omega_0 + q \Delta\omega) \quad (5.22)$$

$$= \sum_{j=-n/2}^{n/2-1} x_{k,l}(j) e^{-2\pi i j (-2pk/(nm) - 2ql/(nm))} \quad (\text{according to step 6}) \quad (5.23)$$

$$= \sum_{j,v,w=-n/2}^{n/2-1} I(j, v, w) e^{-2\pi i k v / m} e^{-2\pi i l w / m} e^{-2\pi i j (-2pk/n - 2ql/n) / m} \quad (5.24)$$

$$= \hat{I}(-2pk/n - 2ql/n, k, l), \quad (5.25)$$

where Eq. (5.24) follows from Eq. (5.23) by using Eq. (5.18).

According to Theorem 4.1 we have that

$$\hat{P}_{x(2p/n, 2q/n)} I(k, l) = \hat{I}(-2pk/n - 2ql/n, k, l) \quad (5.26)$$

and by combining Eqs. (5.25) and (5.26) we obtain

$$\text{Res}_x(p, q, k, l) = \hat{P}_{x(2p/n, 2q/n)} I(k, l). \quad \square \quad (5.27)$$

5.2.3. Complexity of computing the discrete X-ray transform (Algorithm 5.2.1)

We analyze the complexity of computing $\widehat{P}_x I$ (Algorithm 5.2.1). The complexity of computing $\widehat{P}_y I$ and $\widehat{P}_z I$ is the same.

Step 1 of Algorithm 5.2.1 requires $O(n^3)$ operations as it doubles the size of a 3D image of size n^3 by zero padding each direction. Step 2 requires the application of $O(n^2)$ 1D FFTs along the z direction and $O(n^2)$ 1D FFTs along the y direction. Since each FFT application requires $O(n \log n)$ operations, this accounts to a total of $O(n^3 \log n)$ operations.

Next, for fixed $k, l,$ and $p,$ steps 5–7 require $O(n \log n)$ operations, since the most expensive operation is to compute the CZT (chirp Z-transform) in step 7, which requires $O(n \log n)$ operations. This accounts to a total of $O(n^4 \log n)$ operations for the processing of all values of $k, l,$ and $p.$ Hence, computing $\widehat{P}_x I$ requires $O(n^4 \log n)$ operations.

Note that Algorithm 5.2.1 computes $\widehat{P}_x I$ for all directions p and $q.$ If for some application not all directions are needed, they can be discarded from the computation, reducing the complexity of Algorithm 5.2.1.

6. Invertibility

We will show that the samples of the discrete X-ray transform, given in Eq. (4.6), are sufficient to uniquely recover the underlying image $I.$ Since there is a one-to-one correspondence between the discrete X-ray transform of an image I and its Fourier transforms $\widehat{P}_x I, \widehat{P}_y I,$ and $\widehat{P}_z I,$ it is sufficient to show that given the Fourier transform samples $\widehat{P}_x I, \widehat{P}_y I,$ and $\widehat{P}_z I,$ we can uniquely recover the underlying image $I.$

We will use the following lemma, which states that the chirp Z-transform, defined in Section 5.1, is invertible.

Lemma 6.1. *The $n + 1$ samples $\widehat{I}(l), l = -n/2, \dots, n/2,$ of the polynomial*

$$\widehat{I}(l) = \sum_{j=-n/2}^{n/2} c_j e^{-2\pi i j \omega_l}, \tag{6.1}$$

where $\omega_l = \omega_0 + l \Delta\omega, \Delta\omega \neq 0,$ uniquely determine $c_j, j = -n/2, \dots, n/2.$

The proof of Lemma 6.1 is trivial and therefore we omit it.

We begin by inspecting the Fourier samples $\widehat{P}_z I.$ According to Eq. (4.10), for a z -line defined by the parameters (p, q, k, l) we have

$$\widehat{P}_z I(p, q, k, l) = \widehat{I}(k, l, -2pk/n - 2ql/n) \tag{6.2}$$

$$= \sum_{u,v,w=-n/2}^{n/2-1} I(u, v, w) e^{-2\pi i ku/m} e^{-2\pi i lv/m} e^{-2\pi i (-2pk/n - 2ql/n)w/m} \tag{6.3}$$

$$= \sum_{w=-n/2}^{n/2-1} \widehat{I}_{xy}(k, l, w) e^{-2\pi i (-2pk/n - 2ql/n)w/m}, \tag{6.4}$$

where

$$\hat{I}_{xy}(k, l, w) = \sum_{u=-n/2}^{n/2-1} \sum_{v=-n/2}^{n/2-1} I(u, v, w) e^{-2\pi i k u/m} e^{-2\pi i l v/m} \tag{6.5}$$

is the DFT of I in the x and y directions, and Eq. (6.3) follows from Eq. (6.2) by using Eq. (3.16). For fixed p, k , and l and a variable q , we can rewrite Eq. (6.4) as

$$\hat{P}_z I(p, q, k, l) = \sum_{w=-n/2}^{n/2-1} \hat{I}_{xy}(k, l, w) e^{-2\pi i (\omega_0 + q \Delta\omega) w}, \tag{6.6}$$

where $\omega_0 = -2pk/(nm)$ and $\Delta\omega = -2l/(nm)$. According to Lemma 6.1, for fixed k and l , such that $l \neq 0$, we can recover $\hat{I}_{xy}(k, l, w)$, $w = -n/2, \dots, n/2 - 1$. If we repeat this process for all k and l such that $l \neq 0$, we recover $\hat{I}_{xy}(k, l, w)$ for all the Cartesian grid points except the plane $l = 0$. Similarly, if we rewrite Eq. (6.4) as

$$\hat{P}_z I(p, q, k, l) = \sum_{w=-n/2}^{n/2-1} \hat{I}_{xy}(k, l, w) e^{-2\pi i (p \Delta\omega + \omega_0) w}, \tag{6.7}$$

where $\omega_0 = -2ql/(nm)$ and $\Delta\omega = -2k/(nm)$, we can recover, according to Lemma 6.1, $\hat{I}_{xy}(k, l, w)$ for all $k \neq 0$. Therefore, we can recover $\hat{I}_{xy}(k, l, w)$ for all the Cartesian grid points except the line $k = l = 0$, i.e., except the ray in the z direction $\hat{I}(0, 0, w)$. Hence, by applying 1D DFT in the z direction we recover \hat{I} , the 3D DFT of I , from \hat{I}_{xy} on all grid points except the line $(0, 0, w)$. We denote this set of points recovered from \hat{I} by \hat{I}_1 .

We next inspect the Fourier samples $\hat{P}_y I$. According to Eq. (4.9), for a y -line with parameters (p, q, k, l) we have

$$\hat{P}_y I(p, q, k, l) = \hat{I}(k, -2pk/n - 2ql/n, l) \tag{6.8}$$

$$= \sum_{u, v, w=-n/2}^{n/2-1} I(u, v, w) e^{-2\pi i k u/m} e^{-2\pi i (-2pk/n - 2ql/n) v/m} e^{-2\pi i l w/m} \tag{6.9}$$

$$= \sum_{v=-n/2}^{n/2-1} \hat{I}_{xz}(k, v, l) e^{-2\pi i (-2pk/n - 2ql/n) v/m}, \tag{6.10}$$

where

$$\hat{I}_{xz}(k, v, l) = \sum_{u=-n/2}^{n/2-1} \sum_{w=-n/2}^{n/2-1} I(u, v, w) e^{-2\pi i k u/m} e^{-2\pi i l w/m} \tag{6.11}$$

is the DFT of I in the x and z directions. If we rewrite Eq. (6.10) for fixed p, k , and l , we obtain

$$\hat{P}_y I(p, q, k, l) = \sum_{v=-n/2}^{n/2-1} \hat{I}_{xz}(k, v, l) e^{-2\pi i (-2pk/n - 2ql/n) v/m} = \sum_{v=-n/2}^{n/2-1} \hat{I}_{xz}(k, v, l) e^{-2\pi i (\omega_0 + q \Delta\omega) v}, \tag{6.12}$$

where $\omega_0 = -2pk/(nm)$ and $\Delta\omega = -2l/(nm)$. By applying Lemma 6.1 to Eq. (6.12) for fixed k and l , we can recover $\hat{I}_{xz}(k, v, l)$ for $v = -n/2, \dots, n/2 - 1$. If we repeat this process for all k and l such that $l \neq 0$, we recover $\hat{I}_{xz}(k, v, l)$ for all $l \neq 0$. Now, if we rewrite Eq. (6.10) for fixed q, k , and l as

$$\hat{P}_y I(p, q, k, l) = \sum_{v=-n/2}^{n/2-1} \hat{I}_{xz}(k, v, l) e^{-2\pi i(-2pk/n-2ql/n)v/m} = \sum_{v=-n/2}^{n/2-1} \hat{I}_{xz}(k, v, l) e^{-2\pi i(p\Delta\omega+\omega_0)v}, \tag{6.13}$$

where $\omega_0 = -2ql/(nm)$ and $\Delta\omega = -2k/(nm)$, then, we can recover $\hat{I}_{xz}(k, v, l)$ for $v = -n/2, \dots, n/2 - 1$. Again, by repeating the process for all k and l such that $k \neq 0$, we recover $\hat{I}_{xz}(k, v, l)$ for all $k \neq 0$. Therefore, by combining the last two arguments, we recover \hat{I}_{xz} on all grid points except the line $\hat{I}_{xz}(0, v, 0)$. Hence, by applying 1D DFT in the y direction we recover \hat{I} from \hat{I}_{xz} on all grid points except the line $(0, v, 0)$. We denote this set of points recovered from \hat{I} by \hat{I}_2 . If we combine \hat{I}_1 and \hat{I}_2 we recover \hat{I} on the entire grid except the origin. At the origin we have

$$\hat{P}_z I(0, 0, 0, 0) = \sum_{u=-n/2}^{n/2-1} \sum_{v=-n/2}^{n/2-1} \sum_{w=-n/2}^{n/2-1} I(u, v, w) = \hat{I}(0, 0, 0). \tag{6.14}$$

To conclude, we showed that given the Fourier transform samples of the discrete X-ray transform we can recover \hat{I} , the 3D Fourier transform of the image I , and, therefore, we can recover the image I .

7. Conclusions and future research

We presented a definition of the discrete X-ray transform for discrete images. The presented transform does not use an arbitrary interpolation scheme and its parameters are carefully chosen to preserve geometric fidelity (summation along straight geometric lines). It obeys the discrete Fourier slice theorem that allows exact frequency domain analysis with no frequency domain interpolation. Computation of the discrete X-ray transform that is based on the discrete Fourier slice theorem requires no interpolation and uses only 1D frequency domain operations (1D FFTs). This allows efficient implementation using existing 1D tools. An interesting property of the discrete X-ray transform is that it is not limited to 3D and can be easily extended to higher dimensions. All the properties proved for the 3D case exist also in higher dimensions.

We showed that our definition of the discrete X-ray transform is invertible. Analysis of a rapid inversion algorithm is yet to be done as well as investigation of the applicability of such algorithm to physical problems. Computerized tomography is a typical problem where the existing 3D inversion algorithms are inexact and have high complexity.

The forward X-ray transform, which we presented in this paper, has many interesting applications. For example, it enables to perform volumetric directional processing of images in applications such as Fourier volume rendering [10,11], which allows to reduce the complexity of exact slice visualization of a 3D object by almost an order of magnitude. This is in contrast to current implementations, which require frequency domain interpolation that causes artifacts in the reconstructed images. By employing our exact X-ray transform, we do not use any frequency domain interpolations and this leads to both fast and exact slice-visualization algorithms.

References

- [1] A.C. Kak, M. Slaney, Principles of computerized tomographic imaging, in: *Classics in Applied Mathematics*, SIAM, University City Science Center, Philadelphia, PA, 2001.
- [2] S.R. Deans, *The Radon Transform and Some of Its Applications*, Krieger Publishing, revised ed., 1993.
- [3] A.K. Jain, *Fundamentals of Digital Image Processing*, Chapter 10, Prentice Hall, 1989, pp. 431–475.
- [4] F. Natterer, The mathematics of computerized tomography, in: *Classics in Applied Mathematics*, SIAM, University City Science Center, Philadelphia, PA, 2001.
- [5] Y. Shkolnisky, A. Averbuch, D.L. Donoho, M. Israeli, The 2-D discrete Radon transform, in preparation.
- [6] Y. Shkolnisky, A. Averbuch, 3D Fourier based discrete Radon transform, *Appl. Comput. Harmon. Anal.* 15 (1) (2003) 33–69.
- [7] L.R. Rabiner, R.W. Schafer, C.M. Rader, The chirp Z-transform algorithm, *IEEE Trans. Audio Electroacoustics* AU (17) (1969) 86–92.
- [8] L.R. Rabiner, B. Gold, *Theory and Applications of Digital Signal Processing*, Prentice Hall, 1975.
- [9] A.V. Oppenheim, R.W. Schafer, *Discrete time signal processing*, in: *Prentice Hall Signal Processing Series*, second ed., Prentice Hall, 1998.
- [10] T. Malzbender, Fourier volume rendering, *ACM Trans. Graph.* 12 (3) (1993) 233–250.
- [11] B.B. A Lichtenbelt, Fourier volume rendering, Technical report, Hewlett Packard Laboratories, November 1995.